Physics with CDF

S. Miyashita
University of Tsukuba
Ibaraki, Japan

1. Introduction

The success of $S\bar{p}pS$ detectors in isolating interesting parton-parton collisions clearly from the less interesting beam-beam background has made the prospect of TeV-I physics even more exciting because of the higher energy and higher luminosity that TeV-I is designed to deliver.

We indeed have a long list of important physics with CDF, even before the proposed implementation of the small angle detector, the vertex detector, and the super toroid[1]:

1. Elastics and Diffractives
2. Minimum bias events
3. High P_T jets
4. Low P_T, but high $\sqrt{\hat{s}}$ jets
5. Multijet spectroscopy
6. $W^{\pm}$, $Z^0 \rightarrow$?
7. Pair production of gauge bosons
8. Heavy quarks and Technicolor
9. SUSY

It is not my intention, however, to go through the list and discuss the expectation and the limitation of CDF in studying each item in the list. Rather, I will discuss those which are possible only at the higher energy and higher luminosity. Among those are testing the gauge structure of the electro-weak interaction, probing the compositeness scale of quarks, and studying W-decay channels with increased statistics.

In order to show how well CDF can handle these questions, a Monte Carlo programme[2] is used to compute cross sections and generate events. Table I shows cross sections for major physical processes at three different energies.

QCD processes and intermediate vector boson (IVB) productions grow with the machine energy, but the double IVB productions reach a plateau around TeV-I energy. Quite clearly, TeV-I can fill in the gap created between $S\bar{p}pS$ and

LHC and/or SSC, once the designed luminosity of $10^{31}cm^{-2}sec^{-1}$ is reached. Here we assume, however, the luminosity of 10^{30} and the integrated luminosity of 10^{37}.

2. Probing the compositeness scale of quarks

Because the parton-parton scattering obeys the Rutherford formula, it is extremely hard to observe high P_T jets. The limit of P_T at CDF is about 300 GeV (See Fig. 1). Shown also in the figure is the P_T cross section when an additional contact interaction exists. It would be extremely hard to exploit the compositeness scale Λ_c beyond 1 TeV in the P_T distribution.

CERN limit of $\Lambda_c > 300$ GeV is reported by D. Froidevaux in this conference. This limit, however, can be pushed further to 2 TeV if one looks at the invariant mass distribution of final state partons.

This is shown in Figure 2. Jets are mostly found in the rapidity range $2.0 < |\eta| < 4.0$, where the energy flow from the beam-beam background starts rising rapidly. Energy flows due to partons and the beam background are shown in Fig. 3 for the partons CM energy of 1 TeV. Parton jets are seen over the background by more than an order of magnitude even in this integrated energy flow.

As the parton energy decreases, the peak will shift towards lower rapidity range and at the same time the peak height will diminish. Therefore, isolating jets from the background on event by event basis becomes easier as the energy of parton increases.

In Table II, we summarized jet energy resolutions and invariant mass resolutions due to jet-finding algorithm and calorimetry. Since the uncertainty due to the jet-finding algorithm depends very much on jet fragmentation Monte Carlo and we use a rather clean fragmentation scheme, this part can be bigger than the calorimetry resolution. Fig. 4 shows reconstructed jets with window algorithm of $|\eta| \leq 1.0$ and $|\phi| \leq 1.0$.

The Drell-Yan cross section is shown in Fig. 5. It is obvious that even with integrated luminosity of $10^{38}cm^{-2}$ the prospect of seeing a deviation due to the non-elementarity of leptons is rather dim.

On the other hand, heavy objects decaying into lepton pairs may be observable in mass up to 120 GeV, while those decaying into quarks can be seen up to 1 TeV.

3. Pair production of gauge bosons

C. Quigg[3] pointed out that the cross sections given in Table I may be an overestimate. According to his computation within $|\eta| < 2.5$,

$$\sigma(W^+W^-) = 7 \times 10^{-36} cm^2$$

$$\sigma(W^{\pm} Z) = 10^{-36} cm^2$$

$$\sigma(Z\ Z) = 8 \times 10^{-37} cm^2$$

Since the rapidity distributions of W bosons and decay products (leptons or quarks) from W show few events beyond $\eta = 4.0$ (our present calorimetry limit), almost all pair productions are observable at CDF. If we take four jets, or a lepton and two jets final states which account for more than 90 % of W^+W^- events, we expect $170 \sim 70$ events.

4-jet final states are distinctive, in which all 4 jet momenta are quite energetic. The average energies of individual jets are in decending order $E_1 = 118$ GeV, $E_2 = 85$ GeV, $E_3 = 55$ GeV, and $E_4 = 39$ GeV. They can be translated in P_T as 49 GeV, 48 GeV, 35 GeV, and 25 GeV, respectively. Obviously, multijet trigger is needed to reduce QCD background, but we can not be sure of the trigger rate at various P_T thresholds unless we have a multijet QCD generator, namely $2 \to 3$, $2 \to 4$, etc..

As for the signal, W masses can be reconstructed by the combination of jet 1 and jet 4, and jet 2 and jet 3. This is shown in Figs. 6a-b. All events outside the W peak are wrong-combination W's, which do not happen in case where one of the W's decays leptonically. Figs. 6c-d show those after rearranging the combination requiring that at least one W must be in the range of $M_W \pm 20$ GeV. This way we throw away 20 % of good W^+W^- events. They are due to misassignment of hadrons into wrong jet, and thus wrongly reconstructed jets. The later method may be more usefull in discriminating backgrounds. The background comes from both QCD jets and W + jets. If we make a cut at W transverse momentum greater than 30 GeV, we may be able to reduce W + jets events by a factor $\gtrsim 10^{-2}$. We further require that invariant mass of the jets to be in the mass region of W. With an assumption that the invariant mass follows the rule, exp(-4M/E), where E and M are the jet energy and the invariant mass we get another factor 10^{-1} under the W mass peak. This altogether gives a cross section, $2 \times 10^{-35} cm^2$. Similar cut applied for W^+W^- events will reduce the signal to $10^{-35} cm^2 \sim 4 \times 10^{-36} cm^2$. QCD background is harder to estimate.

Just to see the magnitude, we take $\sigma(\rightarrow \text{jets: } P_T > 80 \text{ GeV}) = 10^{-33} \text{cm}^2$. If we require 4 jets and minimum $P_T > 20$ GeV, we get a factor $\sim 10^{-2}$. Further requirement that both invariant masses must fall in the W peak gives another factor 10^{-2}. If this is the case, QCD background may be less serious. In any case background estimation must be done more carefully. Obviously real data must be awaited if one places more confidence on Monte Carlo calculations.

The transverse momentum of W and that of jets decaying from W are shown in Fig. 7.

The average P_T of jets is 40 GeV, and this is the reason for taking $P_T >$ 80 GeV cut in the inclusive P_T distribution of QCD jets when considering QCD background.

4. $W^{\pm}\gamma$ production

The cross section as a function of $W\gamma$ center of mass energy is shown in Fig. 8. If $E_\gamma \geq 50$ GeV is imposed, we get $\sigma = 2.5 \times 10^{-36} \text{cm}^2$. The energy and the transverse momentum of gamma is shown in Fig. 9.

Here, isolation of the gamma from jets is no problem, since they are back to back to each other in the transverse plane, and there is a large rapidity gap between them in the region $E_{W\gamma} > 150$ GeV that we are interested in.

The event topology is clear and distinctive where $\langle E_\gamma \rangle = 120$ GeV and W jets are energetic. Again the background comes mostly from QCD jets and W + jets. We can argue in a similar manner as before that the background level may be manageable. However, in this case we must look at the angular distribution of gammas. This requires more statistics and consequently more difficult than the W^+W^- production study.

The cross section is there for the spectacular observation of these events, and the background may be better understood once we accumulate enough data of multijets, W + jets, etc.. If Quigg's calculation $\sigma(W\gamma;\ E_{W\gamma} > 200 \text{ GeV}) \sim 10^{-37}$ cm^2 is true, then there is even more strong incentives to reach $10^{31} \text{cm}^{-2} \text{sec}^{-1}$ in luminosity.

5. Heavy leptons from W

As is seen in Table I, we expect $\sim 10^5$ W's. This makes TeV-I a W factory in the same sense as LEP and SLC are Z^0 factory. It is all too natural, therefore, to look for various decay modes of W. As an example, I present a case of a heavy lepton decay channel. If the forth generation leptons exist, we expect more than 1000 events decaying into the channel depending of course

on mass of the lepton. The work was done by T. Kamon and Y. Takaiwa at Fermilab, and I present the result.

Since the decay mode,

$$W \to L^{\pm} \nu_L$$

$$\hookrightarrow \ell^{\pm} \nu \nu_L ,$$

may be hard to be separated from $W \to \tau\nu$ channel, we look for hadronic decay of L, specifically

$$L \to j_1 + j_2 + \nu_L .$$

Such events are generated by ISAJET, and the following cuts are applied:

1) lepton veto,

2) $\Sigma E_T^{miss} \geq E_T^{cut}$ (= 10, 15, 20, 25 GeV),

3) $\sum_{tower} |E_T| \leq 120$ GeV,

4) $\cos\theta_{12} = \dfrac{\vec{P}_1 \cdot \vec{P}_2}{P_1 P_2} \geq 0.25$,

5) $\cos\phi_{01} = \dfrac{\vec{P}_0^T \cdot \vec{P}_1^T}{P_0^T P_1^T} \geq -0.6$,

where $\vec{P}_1$, $\vec{P}_2$, and $\vec{P}_0^T$ are momenta of jet 1, jet 2, and missing P_T. Those cuts are chosen to optimize the signal against the background, but not as effective as we wish. The same cuts are applied to generated events, $t\bar{t}$, $b\bar{b}$, and $W \to t\bar{b}$, which make up most of the background. The resulting numbers of events in each category are shown in Table III. Since W reoiles almost always against gluon jets, identification of jet 1 and jet 2 from the heavy lepton is not always unique. Misidentified events shown in Table III are those which are confused with the recoil gluon jet. Mass distributions of the heavy lepton and W are shown for M_L = 30 GeV, and 60 GeV in Figs. 10-11, respectively. Background events are not shown in the figures. Both the mass of W and L are shifted lower. Furthermore, Mjj shows no characteristic peak. This is due to two missing neutrinos in the final state. Nevertheless, if one can identify the parent particle as W in the final state of $j_1 + j_2$ + missing, interpretation of these events is rather unique. Whether or not we can really do that requires more careful studies.

6. Conclusion

The standard model is now established to a surprizing degree by $S\bar{p}pS$. That the observed masses of W and Z come within less than 10 % of the prediction has created more misteries on symmetry breaking mechanism. It is absolutely the must of TeV-I to go beyond the standard model. Since the Higgs discovery seems almost hopeless at CDF, we must look for somewhere else, namely the gauge coupling structure, compositeness, and SUSY. We realize that they are quite a challenge to CDF, but with some luck we hope to see a light out of the standard model.

References

(1) See E. Focardi, A. Menzione, and L. Pondrom in these proceedings.

(2) The programme, called GENF, is originally based on the early version of UA1 Monte Carlo, and is extended later to include many more processes (See CDF Note No. 68, 1980). The difficulty in reproducing both the particle multiplicity and the inclusive single-hadron P_T distribution correctly by KNO is avoided by inclusion of soft QCD jets. The rapidity distribution coming from the soft process must be determined such that the resulting rapidity distribution reproduces that of minimum bias events. Other parameters used in the programme are taken from the following literatures:

Quark-parton distribution functions;
J.F. Owens, and E. Reya, Phys. Rev. D17 (1978), 3003

QCD corrections;
A.J. Buras, and K. Gaemers, Nucl. Phys. B132 (1978), 249

$\bar{p}p$ physics;
R.F. Peierls, T.L. Trueman, and L.-L. Wang, Phys. Rev. D16 (1977), 1397

Pair production of gauge bosons;
R.W. Brown, and K.O. Michaelian, Phys. Rev. D19 (1979), 922
R.W. Brown, D. Sahdev, and K.O. Michaelian, Phys. Rev. D20 (1979), 1164

Jet fragmentation;
Feymann-Field, Krzwicki-Pene, and Lund

(3) C. Quigg, private communication. See these proceedings.

Table I

$\bar{p}p$ cross sections (Monte Carlo Calculation)

	540 GeV	2 TeV	40 TeV
Total	66 ± 6 mb	100 mb	215 mb
Elastic and diffractive	22 mb	28 mb	34 mb
Soft	20 mb	30 mb	60 mb
QCD	22 mb	47 mb	121 mb
gg	13 mb	29 mb	80 mb
gq	8 mb	16 mb	36 mb
qq	1 mb	2 mb	5 mb
Single gauge boson production (cm^2)			
Z^0	7.1×10^{-34}	7.2×10^{-33}	1.4×10^{-31}
$Z^0 \to \ell^+\ell^-$	3.1×10^{-35}	3.2×10^{-34}	7.5×10^{-32}
$W^\pm$	2.0×10^{-33}	1.8×10^{-32}	1.9×10^{-31}
$W^\pm \to \ell^\pm\nu$	2.5×10^{-34}	2.2×10^{-33}	2.4×10^{-32}
Double gauge boson production (cm^2)			
$W^\pm\gamma$	9.2×10^{-37}	1.4×10^{-35}	6.2×10^{-35}
W^+W^-	2.5×10^{-37}	1.7×10^{-35}	7.9×10^{-35}
Z^0Z^0	2.1×10^{-38}	1.9×10^{-36}	2.0×10^{-35}
$W^\pm Z^0$	5.6×10^{-38}	4.4×10^{-36}	1.4×10^{-35}

Table II

Jet Energy Resolution

E (GeV)	Uncertainty: Jet finding	Uncertainty: Calorimetry	$\Delta E_{jet}/E_{jet}$
40	4.4 %	9.5 %	10 %
300	2.8 %	3.5 %	4.5 %
500	2.6 %	2.7 %	3.7 %

Invariant Mass Resolution

M (GeV)	Uncertainty: Jet finding	Uncertainty: Calorimeter	$\Delta M/M$
81 (W mass)	4.3 %	4.8 %	6.4 %
600	2.8 %	2.7 %	3.9 %
1000	2.6 %	1.9 %	3.2 %

Table III

Number of Events Detected at $L = 10^{36} cm^{-2}$

		signal		background		
		$M \to L\nu$ $M_L = 30$	$M \to L\nu$ $M_L = 60$	$W \to t\bar{b}$	$t\bar{t}$	$b\bar{b}$
σ(nb)		1.9	1.3	6.2	5.4	1.1×10^3
E_T^{cut} (miss)	10 GeV	132 [60]	132 [43]	43	19	2400
	15 GeV	118 [54]	109 [39]	23	15	225
	20 GeV	93 [45]	78 [29]	9	9	60
	25 GeV	66 [35]	43 [19]	9	4	15

with all cuts

[ ] misidentified events with the cuts

Figure captions

Fig. 1 Transverse momentum distribution of QCD jets. The dotted line indicates that with an additional contact interaction.

Fig. 2 Invariant mass distribution of final state jets in $\bar{p}p \to$ jets + x.

Fig. 3 Energy flow distributions of QCD jets and beam fragmentation. The dotted line shows the energy flow for minimum bias events. QCD jet and the corresponding beam jet energy flows are shown for the invariant mass of 2 jets at 1 TeV.

Fig. 4 Rapidity and azimuthal angle distributions of jet fragmentaion with respect to jet axis. Jets are generated at $\sqrt{\hat{s}}$ = 1 TeV, and $|\eta| \leq 1.0$, $|\phi| \leq 1.0$ are applied.

Fig. 5 Drell-Yan cross sections computed by the Monte Carlo programme.

Fig. 6 Invariant mass distributions of two jets in $\bar{p}p \to W^+W^- \to 4$ jets:
(a) invariant mass distribution of the most and the least energetic jets;
(b) invariant mass distribution of 2^{nd} and 3^{rd} energetic jets;
(c) and (d) are those obtained by requiring at least one invariant mass must fall into $M_W \pm 20$ GeV.

Fig. 7 Rapidity distributions of W's and jets in $\bar{p}p \to W^+W^- \to 4$ jets:
(a) W's, (b) jets from $W \to 2$ jets.

Fig. 8 Cross sections of double intermediate vector boson production as a function of invariant mass.

Fig. 9 P_T and energy distributions of gamma in $\bar{p}p \to W\gamma$ + x.

Fig. 10 Two jets mass and transverse mass distributions in $W \to L\nu_L$ and subsequently $L \to j_1 + j_2 + \nu_L$ when the heavy lepton mass is 30 GeV:
(a) two jets mass distribution,
(b) transverse mass distribution,
(c) scatter plot of two jets mass v.s. transverse mass,
(d) scatter plot of two jets mass v.s. missing transverse momentum.

Fig. 11 The same distributions as Fig. 10 obtained with M_L = 60 GeV.

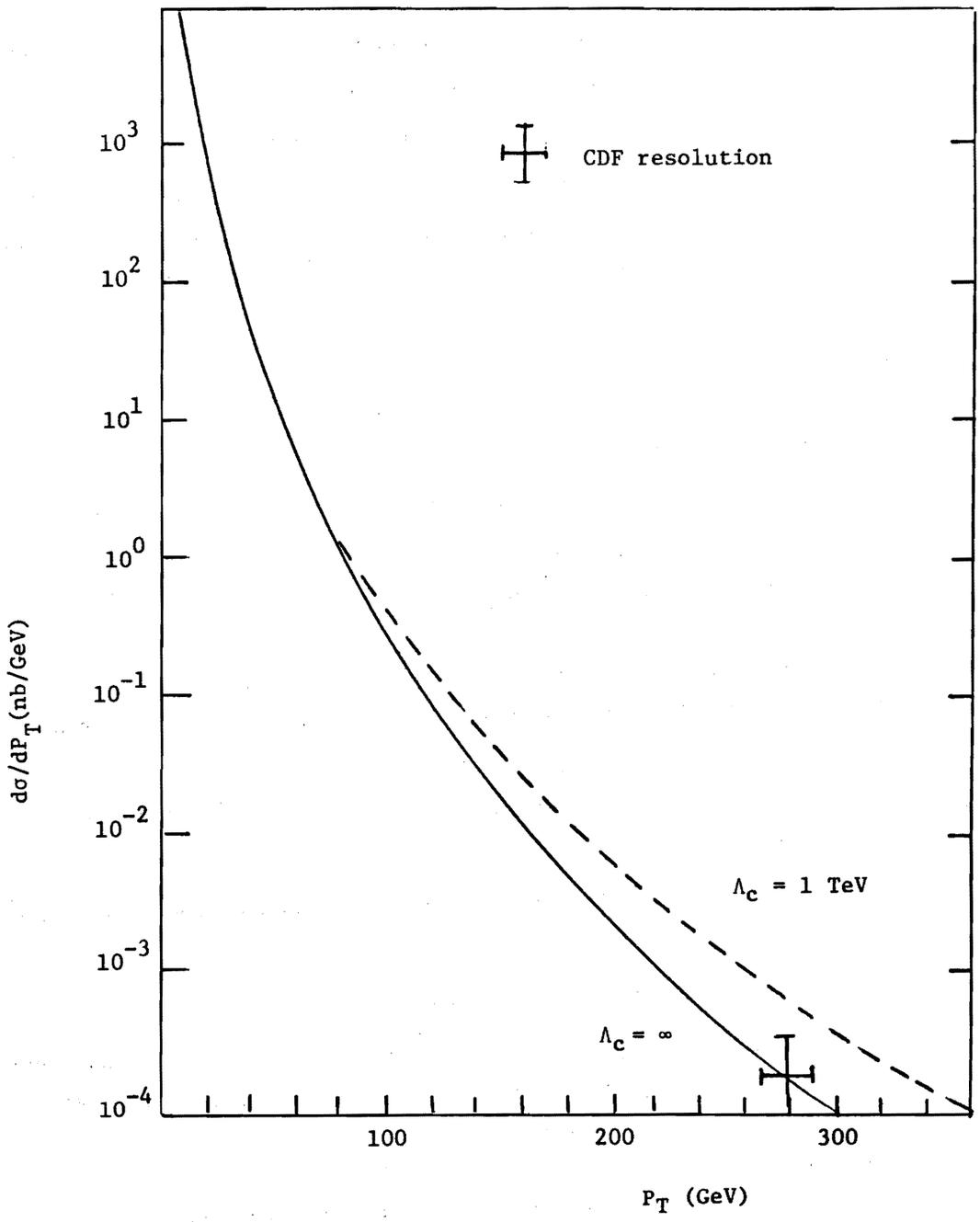

Figure 1

$P_\perp$ distribution of QCD jets

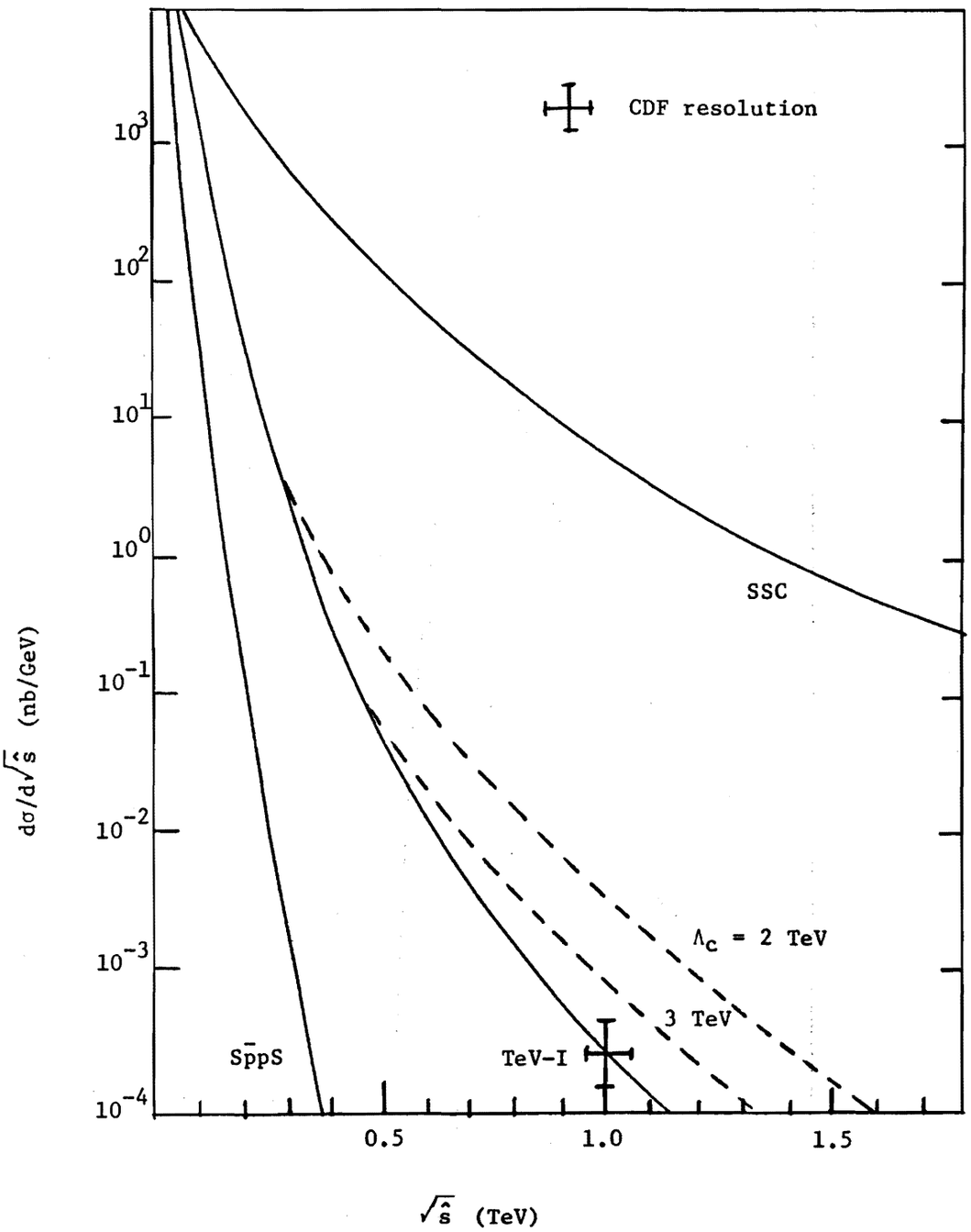

Figure 2

Cross Section of $\bar{p}p \rightarrow$ jets + X as a function of $\sqrt{\hat{s}}$

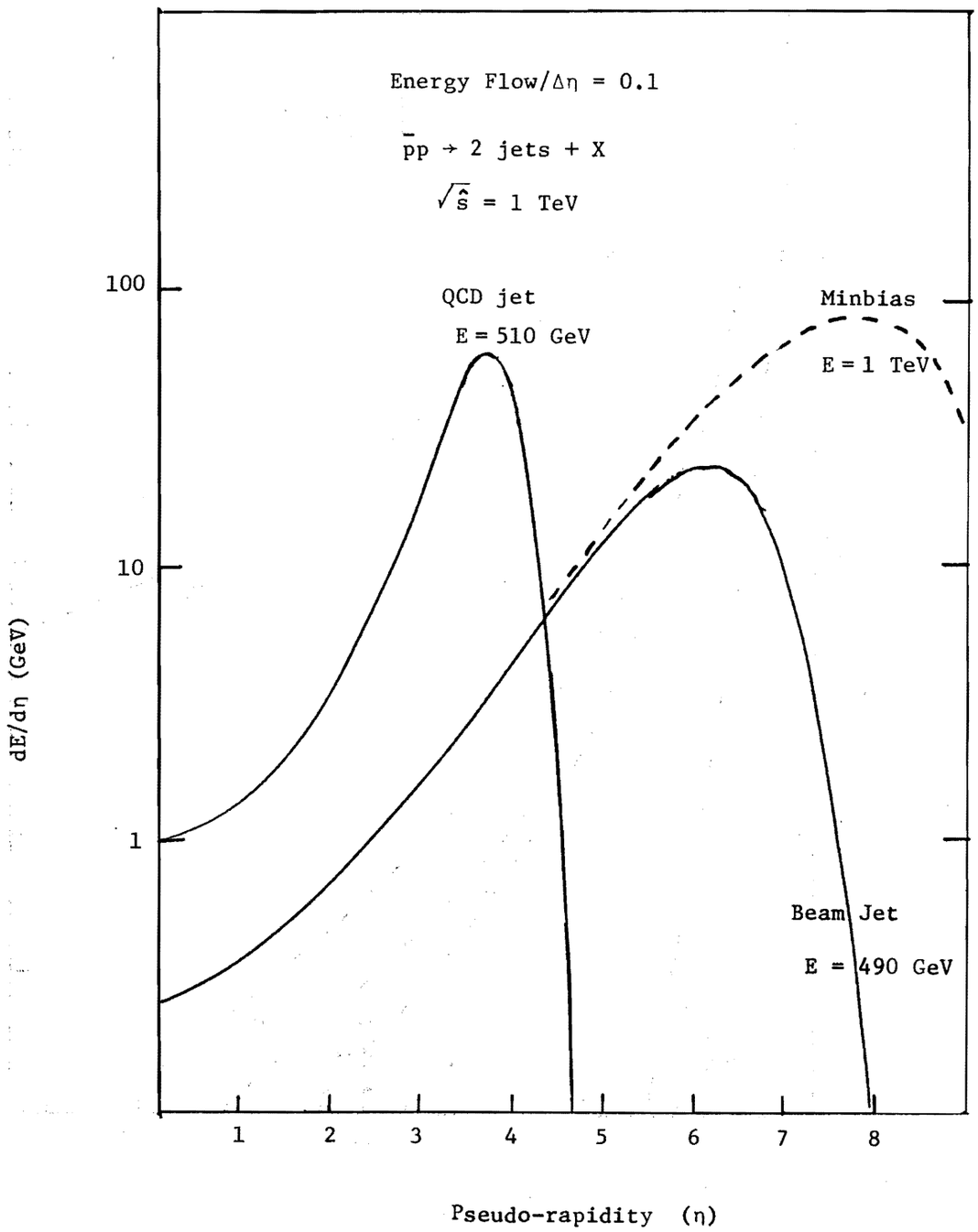

Figure 3

Energy flow distributions

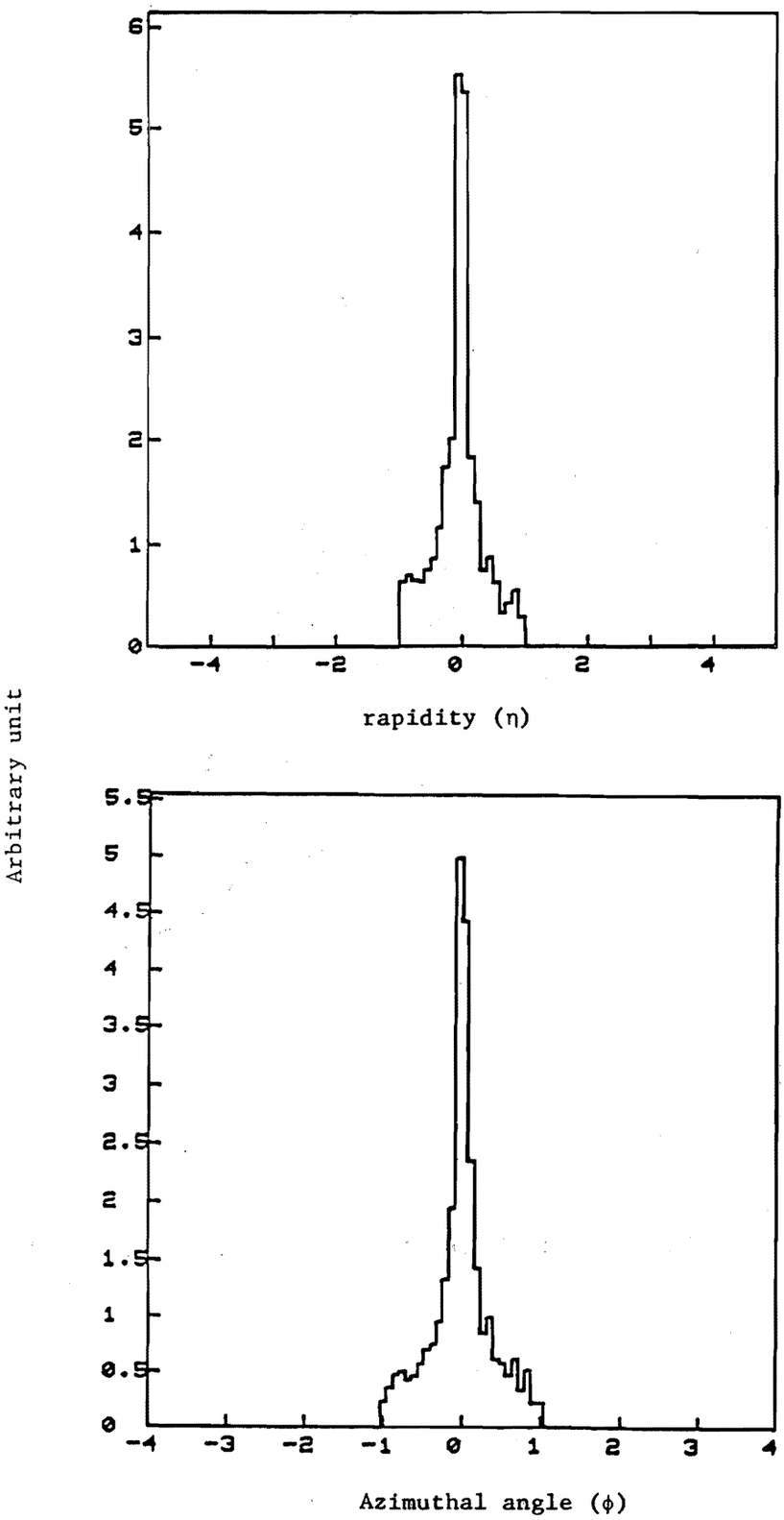

Figure 4

Reconstructed jets

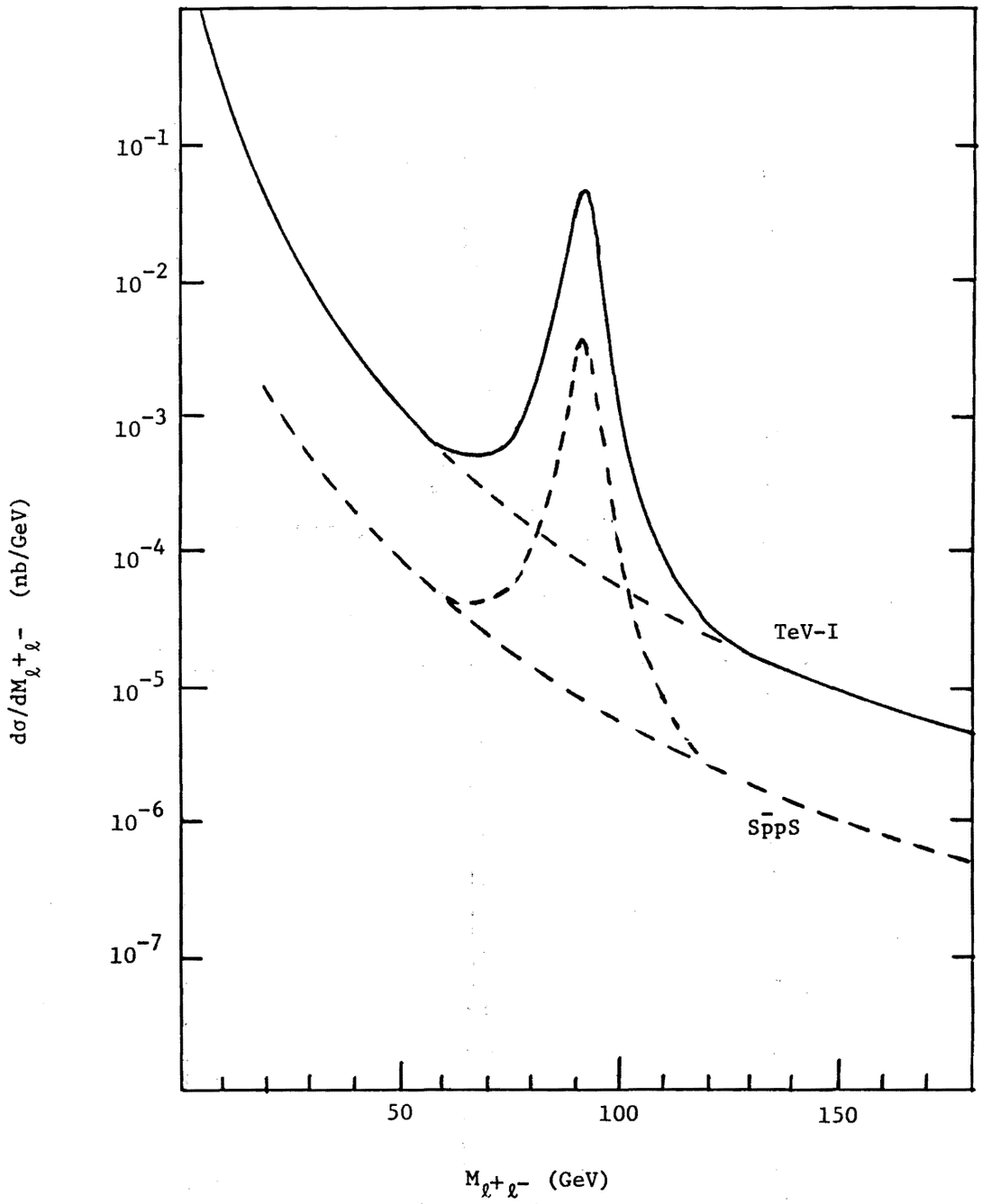

Figure 5

Drell-Yan cross sections

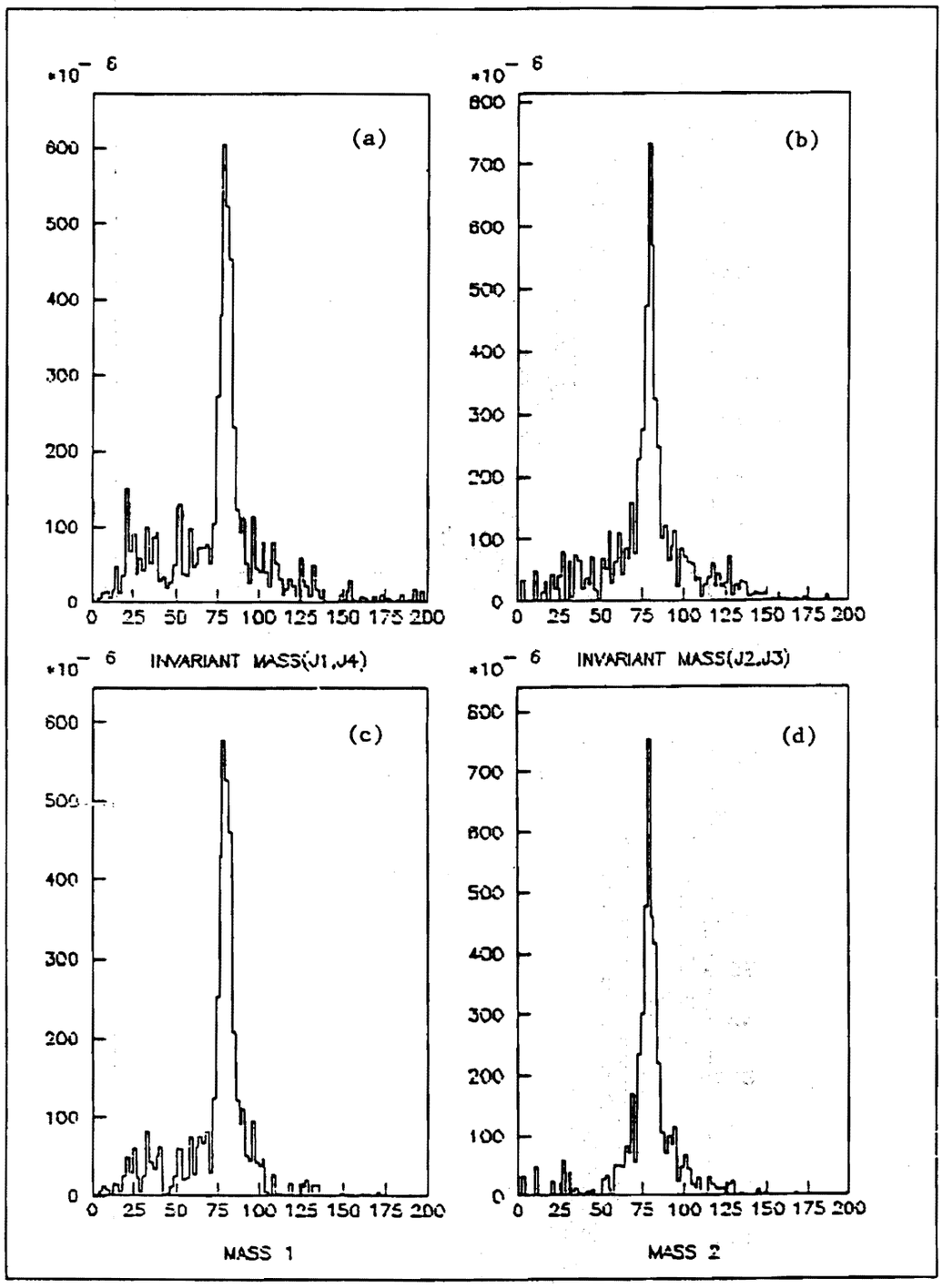

Figure 6

Invariant mass distributions of two jets
in $pp \to W^+W^- \to 4$ jets

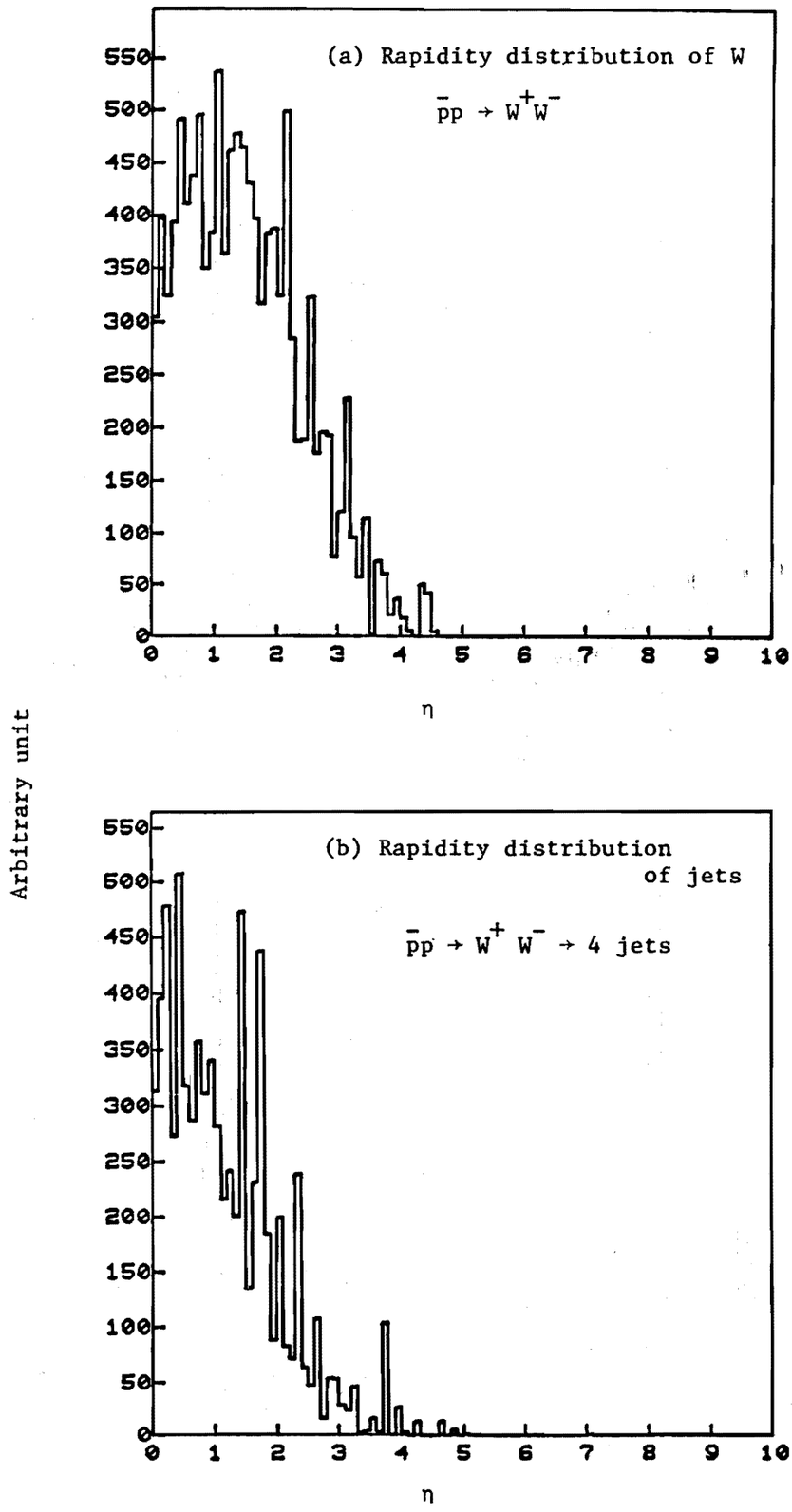

Figure 7

Rapidity distributions of W and jets

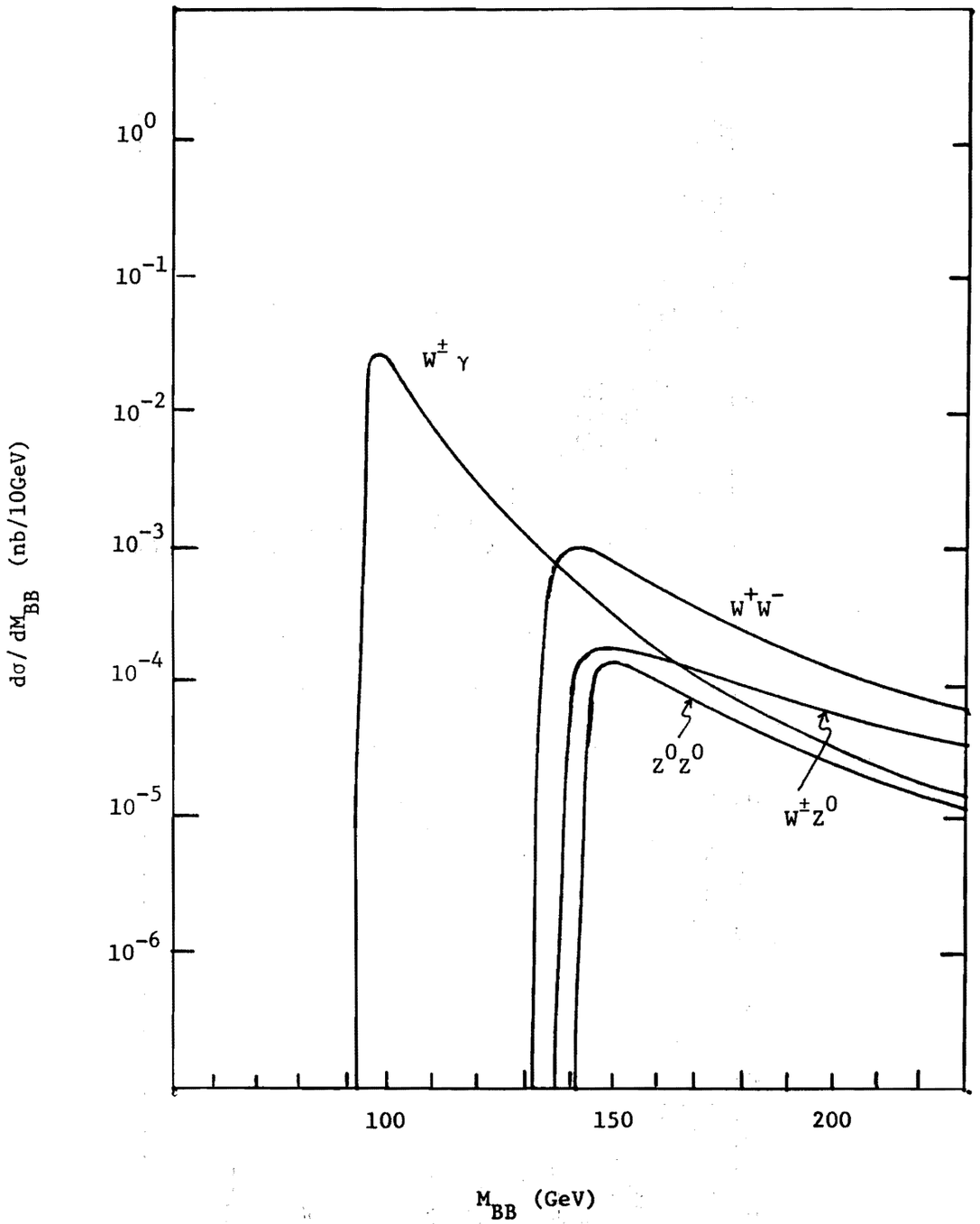

Figure 8

Double IVB productions

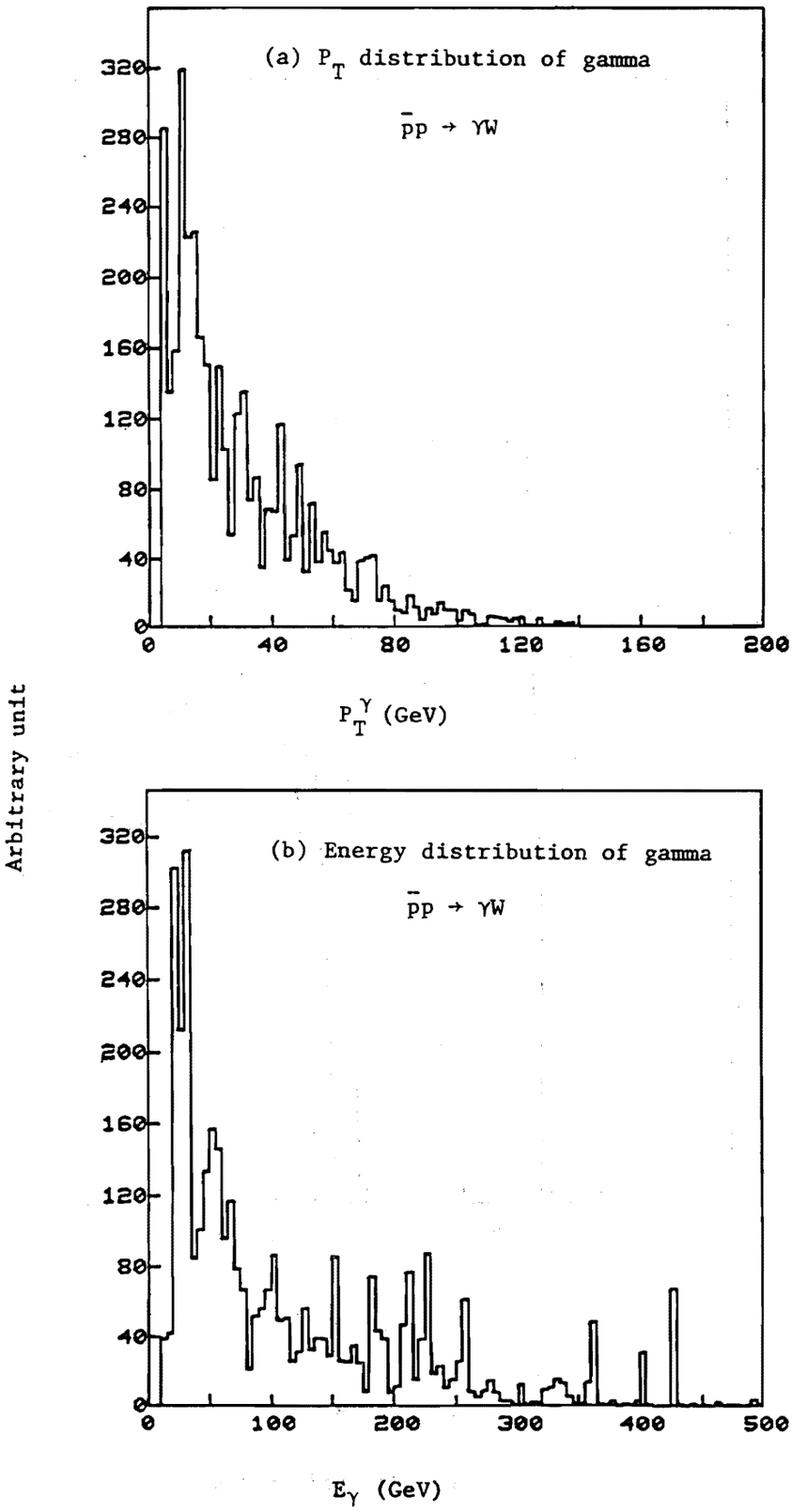

Figure 9

P_T and E distributions of gamma

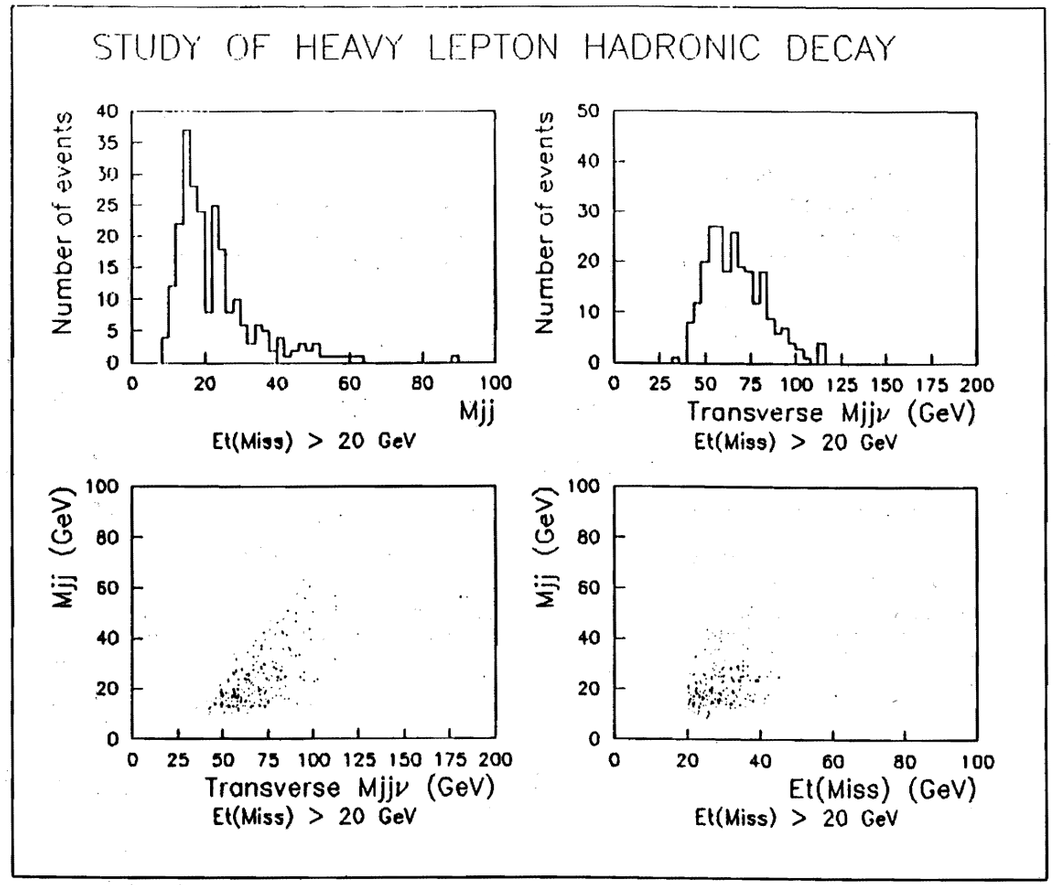

Figure 10

$W \to L \nu_L$; $L \to j_1 + j_2 + \nu_L$ at $M_L = 30$ GeV

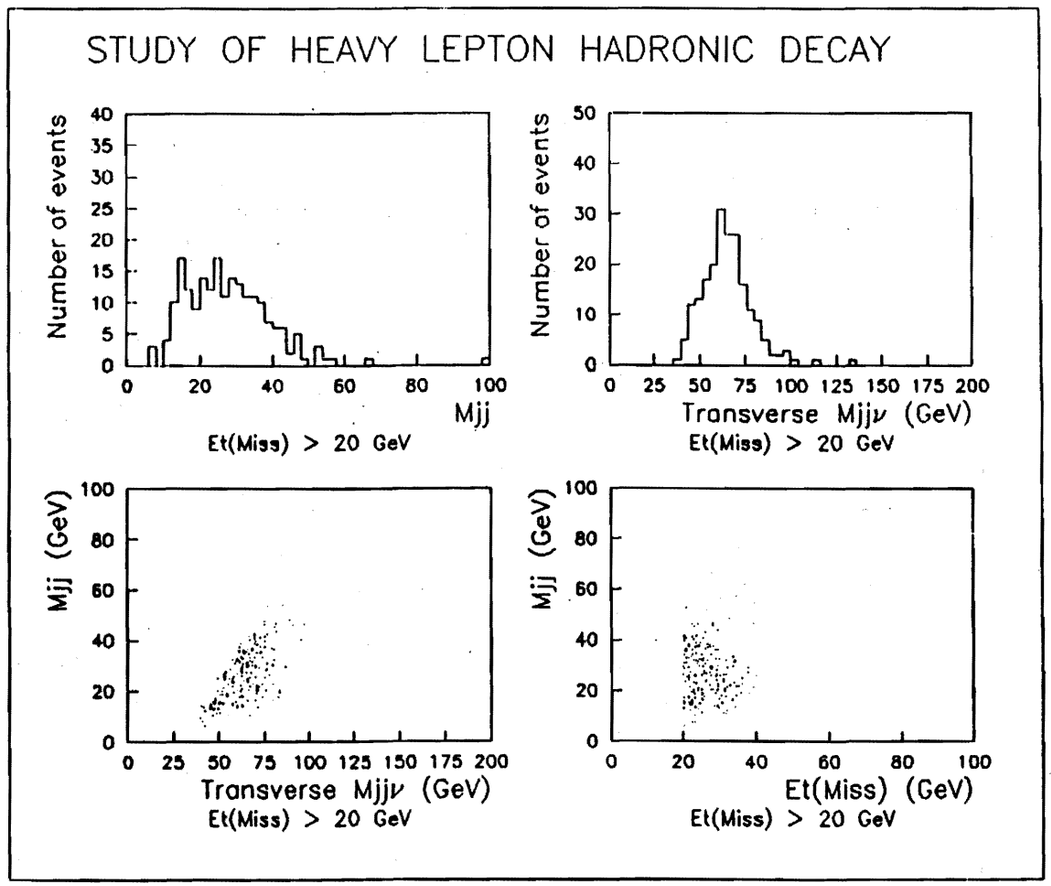

Figure 11

$W \to L \nu_L$; $L \to j_1 + j_2 + \nu_L$ at M_L = 60 GeV